Journal of Membrane Science 543 (2017) 195–201

Contents lists available at ScienceDirect

Journal of Membrane Science

journal homepage: www.elsevier.com/locate/memsci

Sol-gel processed magnesium-doped silica membranes with improved H_2/CO_2 separation

Pelin Karakiliç, Cindy Huiskes, Mieke W.J. Luiten-Olieman, Arian Nijmeijer, Louis Winnubst*

Inorganic Membranes, MESA+ Institute for Nanotechnology, University of Twente, P.O. Box 217, 7500 AE Enschede, The Netherlands

ARTICLE INFO

Keywords:
Magnesium-doping
Microporous silica membrane
Gas separation
Sol-gel

ABSTRACT

Magnesium-doped silica membranes were synthesized and a large increase in H_2/CO_2 permselectivity is achieved as compared to undoped silica membranes. Three magnesium concentrations were studied, namely 10, 15 and 20 mol%, in order to find the optimal Mg-concentration for the highest H_2/CO_2 separation performance. The physical properties of these sol-gel derived Mg-doped silica gels and membranes were characterized by dynamic light scattering, X-ray diffraction and high-resolution scanning electron microscopy. After the incorporation of magnesium into amorphous silica network, the membrane structure remained amorphous. Membrane performance was tested by single gas permeance of He, H_2, CO_2, N_2 and CH_4. With 20 mol% Mg doping, H_2/CO_2 permselectivity values of more than 350 were achieved with a H_2 permeance of 70 $\times$ 10^{-9} mol m^{-2} s^{-1} Pa^{-1}. For pure silica membranes, a H_2/CO_2 permselectivity of 9 was observed with a H_2 permeance of 526 $\times$ 10^{-9} mol m^{-2} s^{-1} Pa^{-1}.

1. Introduction

Membrane separation technology has developed rapidly over recent decades because it is a low-cost and energy-efficient process compared to other separation methods such as pressure swing adsorption and distillation [1]. Ceramic membranes have great potential thanks to their mechanical, thermal and chemical stability [2], which allow them to be used in gas separation applications. Among the ceramic membranes used for gas separation, microporous silica membranes are of great interest due to their uniform and controllable pore size in the sub-nanometer range which makes them an excellent candidate for molecular sieving applications.

Silica membranes are generally synthesized by sol-gel or chemical vapour deposition (CVD) methods [3]. The CVD method provides a denser structure compared to the sol-gel method, resulting in higher selectivity but lower permeability [4–7]. By using the sol-gel method, the pore size can be controlled and a relatively thin (100 nm or less) separation layer can be obtained, which is necessary to achieve high permeability [8–10]. The two main routes in sol-gel synthesis are the colloidal route and the polymeric route [11]. However, for gas separation membranes, which requires pore sizes less than 1 nm, only the polymeric route is applicable. Sol-gel derived microporous silica membranes are fabricated starting from a sol, prepared by an acid-catalysed hydrolysis and subsequent polycondensation of a tetraethyl orthosilicate (TEOS) precursor [12].

Gas separation performance of these membranes have been extensively studied and they show high permselectivities for hydrogen over larger gases such as nitrogen and methane [13]. However, the separation of hydrogen from carbon dioxide remains low and needs to be improved.

Metal doping into the silica network is one of the methods to improve the gas separation performance of these membranes [14–18]. It is often found that after the addition of metals, the membrane structure has become denser, which especially lowers the permeability of larger gases. Also, some metals have a strong interaction with specific gases, which also influences the membrane performance. Igi et al. [14] investigated the effect of cobalt doping into sol gel-derived silica membranes, using tetraethyl orthosilicate (TEOS) as a silica precursor. It was reported that the H_2/N_2 permselectivity increased from 70 to 730 while doping with 33% of cobalt, which shows the great improvement that can be achieved by the addition of a metal. In another study reported by Kanezashi et al. [15], the effect of aluminium doping into bis(triethoxysilyl)methane (BTESM) derived membranes on the membrane performance was investigated. They found that the H_2/CH_4 permselectivity was doubled from 30 to 60 after the addition of 20% aluminium. Another study, investigating the effect of niobium doping into organic linked silica membrane, was reported by Qi et al. [16], who fabricated 25% Nb-doped bis(triethoxysilyl)ethane (BTESE) derived silica membranes. The pure BTESE membrane showed H_2/CO_2 permselectivity of 4, while the Nb-doped membranes resulted in an higher

* Corresponding author.
E-mail address: a.j.a.winnubst@utwente.nl (L. Winnubst).

http://dx.doi.org/10.1016/j.memsci.2017.08.055
Received 10 February 2017; Received in revised form 14 August 2017; Accepted 18 August 2017
Available online 24 August 2017

Table 1
Progresses in gas permselectivities after metal doping into different types of silica membranes.

Ref.	Silica precursor	Metal dopant	Gas components	Permselectivity undoped	Permselectivity metal-doped
[14]	TEOS	33% Co	H_2/N_2	70	730
[15]	BTESM	20% Al	H_2/CH_4	30	60
[16]	BTESE	25% Nb	H_2/CO_2	4	220
[17]	BTESE	9% Zr	H_2/N_2	4	16
			H_2/CO_2	12	100
[18]	TEOS	2.5% Pt	H_2/CO_2	45	70
		0.5/0.5% Mg/Al		45	110

H_2/CO_2 permselectivity of 220. Ten Hove et al. [17] investigated the effect of 9% zirconia doping into BTESE-derived silica membranes and found that the permselectivities of H_2/CO_2 and H_2/N_2 were increased from 4 to 16 and from 12 to 100, respectively. Nijmeijer [18] fabricated pure, 2.5% Pt-doped and 0.5/0.5% Mg/Al-doped TEOS-derived silica membranes and reported that the H_2/CO_2 permselectivities increased from 45 to 70 and 110 as a result of Pt and Mg/Al doping, respectively. All these results show that, in all cases, the ideal separation factors (permselectivities) increased after metal doping as compared to the values obtained by using pure silica membranes. The improved gas permselectivities as a result of metal doping into silica membranes were given in Table 1.

Since metal doping turns the silica structure into a denser network, the increase in the metal dopant loading leads to lower permeances with higher permselectivity values. Boffa et al. [19] fabricated TEOS-derived silica membranes with 25% and 44% Nb-doping and reported that the H_2/CO_2 permselectivity increased from 43 to 70 while the hydrogen permeance reduced by a factor of ten. Similar results were observed in the research reported by Yoshida et al. [20] where TEOS derived silica membranes were doped with zirconia. As the Zr-doping concentration was changed from 10% to 30%, H_2/CO_2 permselectivities increased from 15 to 40 accordingly. However, it was also clear in this research that when the concentration of zirconia was increased further to 50%, the H_2 permeance decreased more significantly than that of CO_2, resulting in a H_2/CO_2 permselectivity of 7.

It is known that alkaline-earth ceramic oxides, such as MgO, have high CO_2 capture capacities over a wide temperature range [21]. By the incorporation of alkaline-earth metals into the silica membrane structure, basic sites are eventually created. The basic sites in amorphous Mg-Al mixed oxides are shown to be capable of adsorbing CO_2 at 200 °C by the given mechanism [22]:

$$Mg - O + CO_2 \rightarrow Mg - O...CO_2(ads)$$

Therefore, we have decided to fabricate and study Mg-doped silica membranes for H_2/CO_2 separation in order to investigate the improvement in the gas separation performance as a result of Mg doping. Furthermore, the influence of dopant concentration was examined by fabricating membranes with three different dopant concentrations. Pure silica membranes without Mg-doping were also prepared for comparison purposes.

To our knowledge, this is the first work that discusses the effect of magnesium doping on the gas separation performance of amorphous silica membranes. It is hoped that it will inspire future studies on alkaline metal doping into silica membranes.

2. Experimental

2.1. Membrane fabrication

Commercially available, polished, α-Al_2O_3 discs (diameter 39 mm, thickness 2 mm, porosity 35% and pore size 80 nm, supplied from Pervatech B.V. the Netherlands) were used as a support. On the top of these α-Al_2O_3 supports, a mesoporous γ-Al_2O_3 layer was applied in order to serve as an intermediate layer between the macroporous α-Al_2O_3 support and the microporous amorphous silica separation layer. The γ-Al_2O_3 layer was prepared by dip-coating the α-Al_2O_3 support into a solution of a colloidal 0.5 M boehmite (γ-AlOOH) (60 vol%) and 0.5 mM polyvinyl alcohol (PVA) solution (40 vol%), followed by calcination at 650 °C for 2 h with a heating and cooling rate of 1 °C/min. The dipping and calcination procedures were performed twice in order to avoid any possible defect formation. Further details of the fabrication of the γ-Al_2O_3 intermediate layer are given in [8].

The procedure for the fabrication of the amorphous silica layer was adapted from the work of De Lange et al. [23]. The silica sol was prepared by an acid-catalysed sol-gel reaction of tetraethyl orthosilicate (TEOS, Sigma Aldrich) in ethanol after the addition of 1 M HNO_3. During the addition of the acid, the TEOS-ethanol solution was put into an ice-bath in order to avoid pre-hydrolysis and stirred continuously to obtain a homogeneous solution. After that, the solution was refluxed under continuous stirring at 60 °C for 3 h. The final mixture has a molar ratio of TEOS/EtOH/H_2O/HNO_3 of 1:3.8:6.2:0.085. After 3 h of reflux, the solution was put into an ice-bath to stop the reaction and diluted 19 times with ethanol to obtain the final dip solution. The γ-Al_2O_3 coated membrane was dipped into the silica dip solution, which had been filtered previously (Schleicher & Schuell, with a pore size of 0.2 μm). Dip-coating was done in a clean room (class 100) using a dip-coater (Velterop DA 3960/02) with an angular dipping rate of 0.06 rad s^{-1}. After that, the dip-coated membranes were put into an air-furnace and calcined at 600 °C for 3 h with a heating and cooling rate of 0.5 °C/min. The calcination temperature was set at 600 °C to obtain the high permselectivity values as suggested by De Vos and Verweij [8]. The dipping and calcining processes were repeated once more in order to minimize the defect concentration on the silica layer.

As a magnesium precursor for the Mg-doped silica, magnesium nitrate hexahydrate ($Mg(NO_3)_2{\cdot}6H_2O$, Sigma Aldrich) was used, which was dissolved into a 1 M HNO_3 solution and added to the TEOS-ethanol solution, and then refluxed at 60 °C for 3 h under continuous stirring. The undiluted 10 mol%, 15 mol% and 20 mol% magnesium-doped silica sols (sample codes resp. $Mg10SiO_2$, $Mg15SiO_2$ and $Mg20SiO_2$) have final molar compositions of TEOS/EtOH/$Mg(NO_3)_2$/H_2O/HNO_3 of 1:3.8:0.11:6.2:0.085, 1:3.8:0.17:6.2:0.085 and 1:3.8:0.25:6.2:0.085, respectively. H_2O originated from $Mg(NO_3)_2{\cdot}6H_2O$ was included for the final molar composition. After the synthesis, the sol was diluted in ethanol in order to obtain the same Si molarity as in the final dip sol of the pure silica. Identical dip-coating/calcination procedures, as applied for pure silica membranes, were used at this stage.

The unsupported pure and Mg-doped silica powders were prepared to be analysed by X-ray diffraction (XRD), gas adsorption and thermogravimetric analysis (TGA). For this reason, the ethanol diluted final dip sol was poured into a petri dish and dried overnight at room temperature. After drying, the flakes were calcined at 600 °C for 3 h under air with a heating and cooling rate of 0.5 °C/min and a dwell of 3 h.

2.2. Characterization

The particle size distribution (PSD) of the sols was determined by the dynamic light scattering (DLS) technique using a Malvern Zetasizer Nano ZS instrument. By means of the DLS technique, the intensity-

weighted PSD is obtained. The crystalline structure of the membranes was analysed by X-ray diffraction using a Bruker D2 Phaser with Cu-Kα radiation (λ = 1.5418 Å). The thickness of the membrane and the morphology of the microporous top layer were determined by using a JEOL JSM 6400 high-resolution scanning electron microscope (HRSEM). CO_2 gas adsorption measurement was performed on unsupported pure and Mg-doped silica powder using Quantachrome Autosorb-1MP at 0 °C. Prior to measurement, the powder was degassed at 300 °C under vacuum for 3 h. Thermogravimetric Analysis (STA 449 F3 Jupiter®, NETZSCH) was used to determine the mass change on the unsupported powders upon the change of gas atmosphere. The calcined powders first heated to 200 °C with 10 °C/min and then kept under N_2 flow for 1 h. Then, the gas flow was changed to CO_2:N_2 (5:2) mixture and the mass changes upon the exposure of CO_2 is recorded.

The gas permeability of the membranes were carried out on a Convergence OSMO single gas permeation set-up, which works in a dead-end mode in which the selective layer of the membrane was exposed to the gas feed. During the measurements, the feed pressure and the permeate pressure were kept at 3 and 1 bar, respectively, which gives a 2 bar transmembrane pressure. The gases were measured in the given order (gas kinetic diameter): He (0.255 nm), N_2 (0.364 nm), CH_4 (0.389 nm), H_2 (0.289 nm) and CO_2 (0.33 nm). The gas permeation data were recorded for each gas when it reached a steady state. The detection limit of the single gas permeance for an applied transmembrane pressure of 2 bar was calculated as 0.2×10^{-9} mol m^{-2} s^{-1} Pa^{-1} using the minimum detectable flow of the mass flow meters. The permselectivity is calculated from the ratio of permeances of single gases. A schematic representation of the experimental set-up is shown in Fig. 1.

3. Results and discussion

The particle size and particle size distribution of the sol are critical parameters for obtaining a defect-free separation layer on the γ-Al_2O_3 intermediate layer. Particles that are too large and/or have a too broad particle size distribution would easily result in defect formation in the layer after calcination, while the particle size must be large enough to be suitable for coating on the γ-Al_2O_3 without penetrating into its pores [23]. The intensity particle size distributions of the various sols are shown in Fig. 2.

The mean average intensity-based particle size of SiO_2, $Mg10SiO_2$, $Mg15SiO_2$ and $Mg20SiO_2$ were calculated as 9.5, 10.5, 12.8 and 13.9 nm, respectively. All the sols were found to be suitable for coating on the intermediate γ-Al_2O_3 layer with a pore size of 5 nm.

The XRD patterns of the pure and Mg-doped silica membranes were analysed to see if any crystal phase is formed in the separation layer after metal doping (see Fig. 3). For comparison, an XRD pattern was also recorded of a γ-Al_2O_3 coated α-Al_2O_3 support. As can be seen from

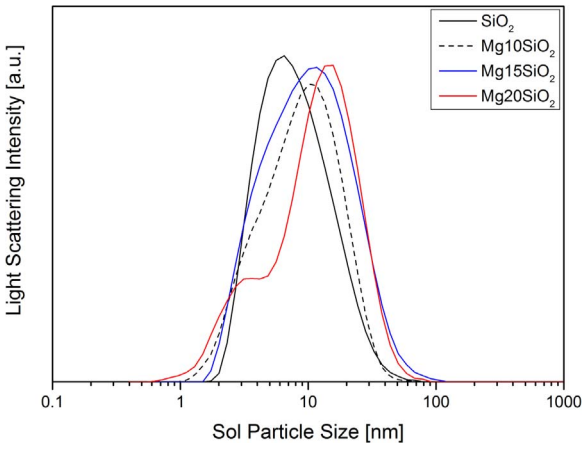

Fig. 2. Dynamic light scattering intensity of particle sizes of the pure and Mg-doped silica sols.

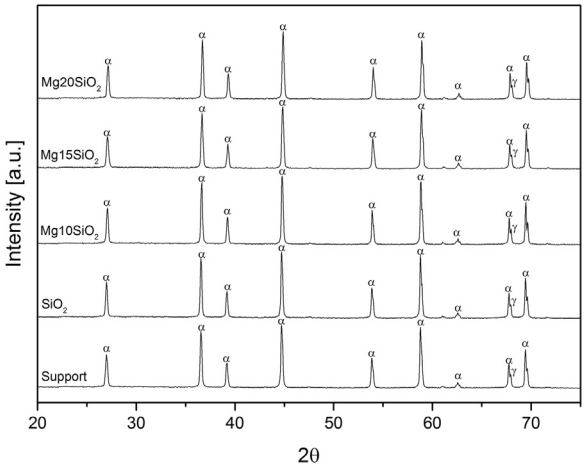

Fig. 3. X-ray diffraction patterns of $Mg20SiO_2$, $Mg15SiO_2$, $Mg10SiO_2$, SiO_2 and the support.

Fig. 3, all five XRD patterns are identical. The XRD patterns only showed signals that could be attributed to the α-Al_2O_3 or γ-Al_2O_3 phase. As the silica is amorphous, it does not give any XRD pattern belonging to the silica structure.

In addition to the XRD analysis of the membranes, where the selective top layer is relatively thin as compared to the support layer, an unsupported 20% Mg-doped silica powder was also analysed. The XRD pattern of this calcined powder, as given in Fig. 4, confirms its

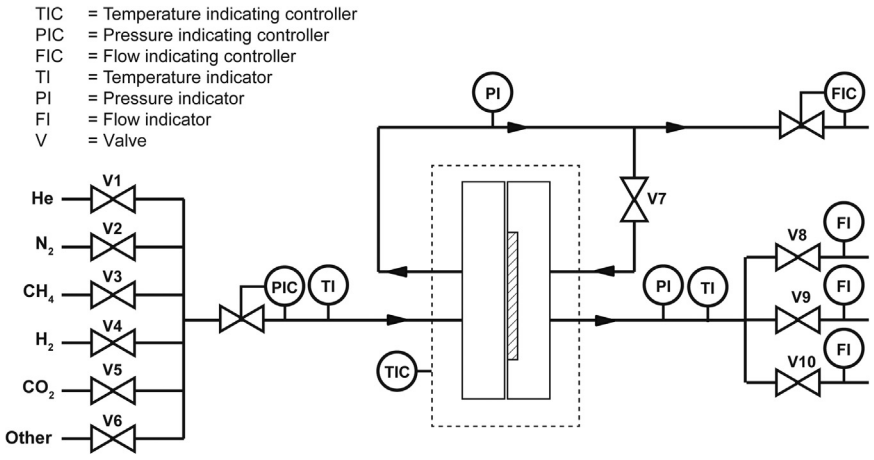

Fig. 1. Schematic representation of the gas permeation set-up.

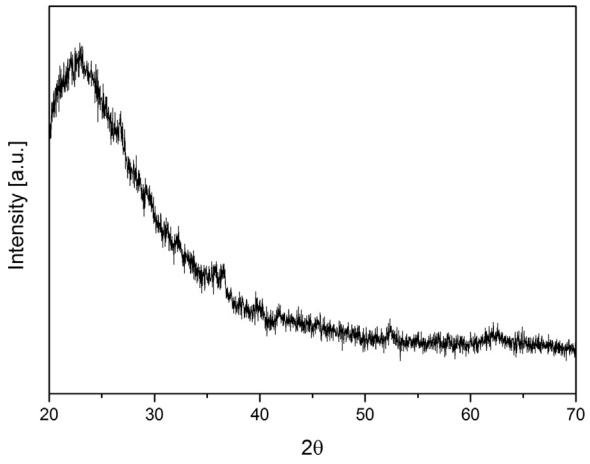

Fig. 4. X-ray diffraction patterns of a calcined 20% Mg-doped SiO2 powder.

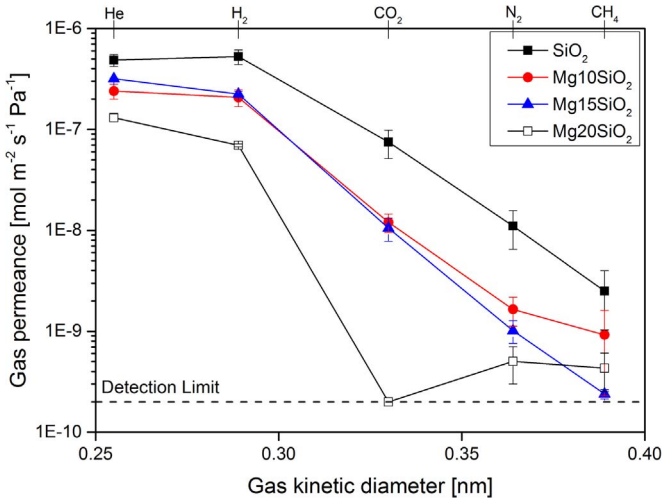

Fig. 6. Gas permeance as a function of gas kinetic diameter for the pure and Mg-doped silica membranes measured at 200 °C and 2 bars transmembrane pressure (lines are a guide to the eye).

amorphous structure and no crystalline phase is formed as a result of magnesium doping.

The surface and cross-sectional morphologies of the pure and Mg-doped silica membranes were analysed by HR-SEM and the results are depicted in Fig. 5.

The boundary between the selective layer and the γ-Al_2O_3 intermediate layer of the support is clearly visible for all membranes, showing no penetration of the selective layer into the pores of intermediate layer. For all membranes, the thicknesses of the γ-Al_2O_3 intermediate layer were found to be identical and within the range of 3.5–3.6 μm. The pure silica membrane shows a homogeneous, smooth and defect-free surface whereas Mg-doped membranes, regardless of the concentration of the doped metal, have some pits distributed all over the membrane surface (see Fig. 5c and d). For all membranes, the thickness of the selective layer was found to be in the range of 65–75 nm. The width of the pits were found to be smaller for lower concentration of magnesium, with diameters varying from 50 to 95 nm for 10% Mg-doped silica, whereas wider pits or even collapsed pits with sizes in the range of 100–400 nm were observed for 20% Mg-doped silica membranes. From the SEM images, the depths of the pits were found to be in the range of 10–20 nm. Hence, a separation layer with a thickness of at least 45 nm is still present at the "bottom" of these pits. Furthermore, a Rhodamine-B test was performed in order to ensure that these pits do not reach the intermediate γ-Al_2O_3 layer, so that there is a continuous silica separation layer lying on the intermediate layer. Rhodamine B solution is used as a staining dye and it gives a pink colour upon contact with the Al_2O_3 layer. A few drops of this solution were poured onto the membranes and, after rinsing the excess solution with ethanol, no pink colour was observed on the membrane surface, indicating that the silica membranes are defect-free and the pits formed

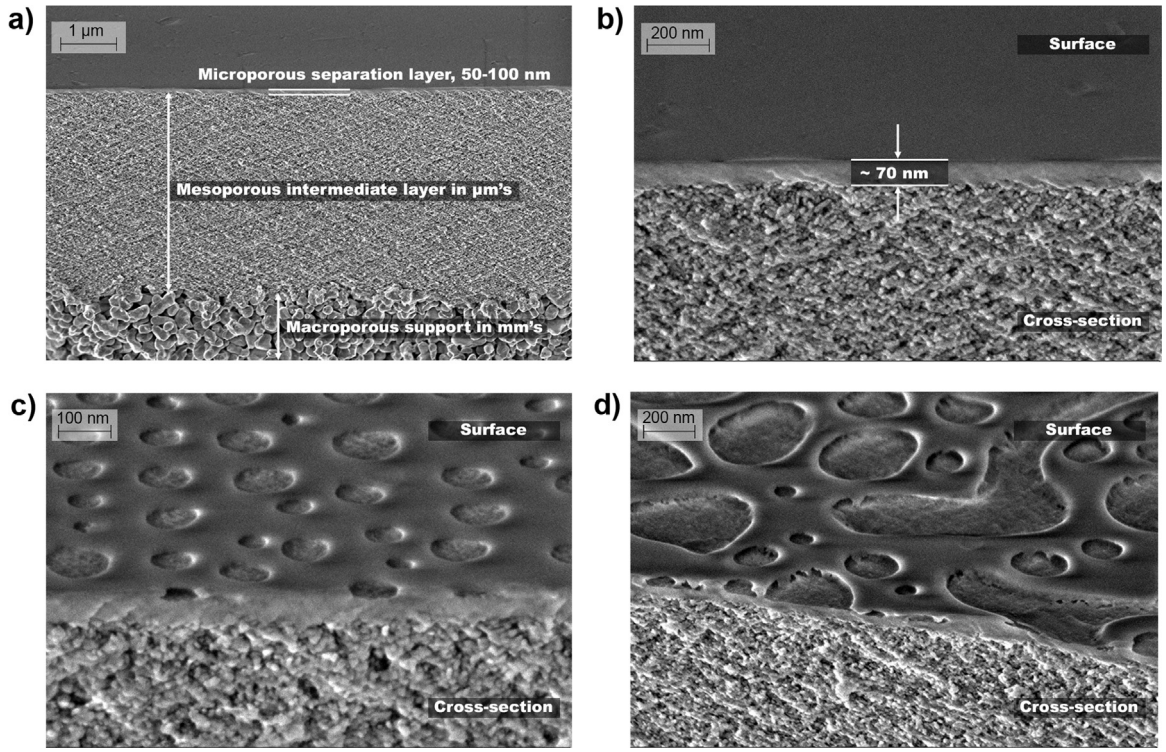

Fig. 5. HRSEM images of several membranes: a) cross-section of SiO_2; b) surface and cross section of SiO_2; c) surface and cross section of $Mg10SiO_2$; and d) surface and cross section of $Mg20SiO_2$.

Table 2
The single gas permeances and H_2/CO_2 permselectivity of both pure and Mg-doped silica membranes at 200 °C and 2 bar.

Membranes	Gas permeance [10^{-9} mol m^{-2} s^{-1} Pa^{-1}]					H_2/CO_2	H_2/N_2
	He	H_2	CO_2	N_2	CH_4		
SiO_2	488 ± 67	526 ± 87	75 ± 23	11 ± 5	3.0 ± 1	9 ± 3	88 ± 35
$Mg10SiO_2$	240 ± 41	210 ± 39	12 ± 2.5	1.6 ± 0.5	0.9 ± 0.6	19 ± 4	164 ± 41
$Mg15SiO_2$	320 ± 6	220 ± 15	11 ± 2.7	1.0 ± 0.2	0.2 ± 0	24 ± 4	249 ± 38
$Mg20SiO_2$	130 ± 12	70 ± 2	*	0.5 ± 0.2	0.4 ± 0.1	> 350	204 ± 45

* Permeances are below the detection limit of the equipment (0.2 × 10^{-9} mol m^{-2} s^{-1} Pa^{-1}).

on the Mg-doped membranes do not reach the intermediate γ-Al_2O_3 layer. Also, the results of gas permeation measurements – as will be discussed later – are an indication that an intact separation layer was present on the membrane surface.

For each composition, four membranes from two sols were fabricated for studying single gas permeation. By using eight membranes for each composition, the reproducibility of the results can be evaluated. Fig. 6 shows the average gas permeances measured at 200 °C at a transmembrane pressure of 2 bars through pure and Mg-doped silica membranes as a function of gas kinetic diameters. The error bars represent the standard error calculated from the standard deviation divided by the square root of number of samples tested. The average gas permeance through each type of membrane is given in Table 2. The permselectivity values were calculated for each single membrane, and these values were averaged. The values given after the plus-minus sign represent the standard errors calculated from the standard deviation of each result from the average values divided by the square root of number of samples analysed.

As shown in Fig. 6 the gas permeances decrease with an increasing gas kinetic diameter as expected as the pores of the separation layer are in the microporous regime. As the gas permeance values decrease with increasing gas kinetic diameter, and the fact that permselectivity values are much higher than the Knudsen selectivities (which are resp. 4.69 for H_2/CO_2 and 3.74 for H_2/N_2), molecular sieving can be regarded as the (main) gas transport mechanisms for all membranes. However, in pure silica, the permeance of H_2 is higher than that of He. As the molecular weight of H_2 (2) is lower than the molecular weight of He (4), it is assumed that Knudsen selectivity is the separation mechanism for these gases in pure silica membranes. This Knudsen selectivity for the relative smaller gases changes to molecular sieving, when Mg is doped to the silica membranes, especially for 15% and 20% Mg-doped silica membranes (see Table 2), which exhibit higher He permeances as compared to H_2.

In general, by the incorporation of magnesium into the amorphous silica network, lower gas permeances are observed, suggesting that the pore structure is denser in this case (see Table 2). This decrease is more pronounced for larger gases which in return results in increased permselectivities of H_2 over the bigger gases (CO_2, N_2 and CH_4). This is an indication that especially the bigger pores (sizes > 0.3 nm) decrease in size and/or amount after doping with Mg. This has already been observed after 10% Mg-doping, where the decreases in CO_2 and N_2 permeances were more pronounced than those for He and H_2 if compared with pure silica resulting in doubling of the of H_2/CO_2 and H_2/N_2 permselectivities compared with undoped silica membranes. Besides, the CH_4 permeance of 0.9 × 10^{-9} mol m^{-2} s^{-1} Pa^{-1} was found to be just above the detection limit of the equipment (0.2 × 10^{-9} mol m^{-2} s^{-1} Pa^{-1}). At an increasing dopant concentration to 15%, the amount and/or size of bigger pores (sizes > 0.3 nm) decrease even more as shown by the almost undetectable methane permeance and increasing H_2/N_2 permselectivity. When the dopant concentration was increased to 20%, there was no detectable CO_2 permeance. None of the eight studied 20% Mg-doped SiO_2 membranes showed any detectable CO_2 permeance, resulting in average H_2/CO_2 permselectivities higher than 350. As several membranes were studied from two sets of sols, the reproducibility of the results on the non-detectable CO_2 permeance and improved H_2/CO_2 permselectivity is demonstrated.

Surprisingly, for these 20% Mg-doped SiO_2 membranes the permeance of larger gases, N_2 and CH_4, were found to be just above the detection limit. Having detectable permeance for the relative bigger gases, N_2 and CH_4, while no permeance for the smaller gas, CO_2, indicates that CO_2 transport may not only be determined by the size of the gas as occurs in the molecular sieving transport but also by the interaction between CO_2 and the 20% Mg-doped silica membrane. This interaction can be due to the available basic sites in alkaline metal oxides, in this case MgO, having a large CO_2 adsorption capacity [21]. When acidic CO_2 molecules pass through the pores, CO_2 starts to be adsorbed on the walls where the basic sites are located. The adsorption of CO_2 narrows the pore openings, avoiding the permeation which results in non-detectable CO_2 flow on the permeate side. This mechanism is described in Fig. 7. As seen, CO_2 permeates easily through the pores of SiO_2 where the pore sizes are below 0.5 nm but still larger than the kinetic diameter of CO_2 (0.33 nm). In $Mg20SiO_2$ membranes, the densification of the Mg-doped silica membrane structure resulted in decreased gas permeances for CO_2, N_2 and CH_4 due to having pores smaller than 0.33 nm. Through the larger pores of $Mg20SiO_2$ (denoted as pore sizes between 0.33 and 0.5 nm in Fig. 7), N_2 and CH_4 were still able to pass through the permeances as can also be seen from their gas permeance values given in Table 2. However, due to the interaction with the basic sites as a result of Mg doping, CO_2 was adsorbed on the pore walls and prevented its own permeation.

In order to show whether CO_2 adsorption is reversible, a second CH_4 single gas permeation was performed after the CO_2 permeation test. As CH_4 is larger than CO_2, CH_4 could not pass through the pores if they were occupied or narrowed as a result of still adsorbed CO_2. However, no decrease in CH_4 permeation was observed. This suggest that all adsorbed CO_2 is removed demonstrating the reversibility of the interaction.

The gas permeances through a 20% Mg-doped silica membrane were also measured at various temperatures (50, 100, 150 and 200 °C) and a transmembrane pressure of 2 bar. These results are given in Fig. 8 and summarized in Table 3. Gas permeances of molecules with small kinetic diameter, such as He and H_2, increase with increasing temperature, suggesting an activated transport mechanism [24]. At each single temperature, no detectable CO_2 permeances were observed. As the H_2 permeance increases with an increasing temperature while CO_2 permeance remains undetectable, a temperature increase leads to an increase in H_2/CO_2 permselectivity. For larger gases such as N_2 and CH_4, the gas permeances were close to the detection limit and did not change as a function of temperature as much as smaller gases did. By showing no detectable CO_2 permeance at each single temperature up to 200 °C, it is proven that the 20% Mg-doped silica membranes exhibited an excellent affinity to CO_2 over a wide temperature range (50–200 °C). Besides, permeance of the bigger, but "inert", gas N_2 was even observed at low temperatures, again indicating the affinity of 20% Mg-doped silica membranes towards CO_2.

CO_2 adsorption measurements on pure and 20% Mg-doped silica powders were performed at 0 °C and the adsorption isotherms were analysed as a function of relative pressure (P_{rel} = P/P_0 where P_0 is the

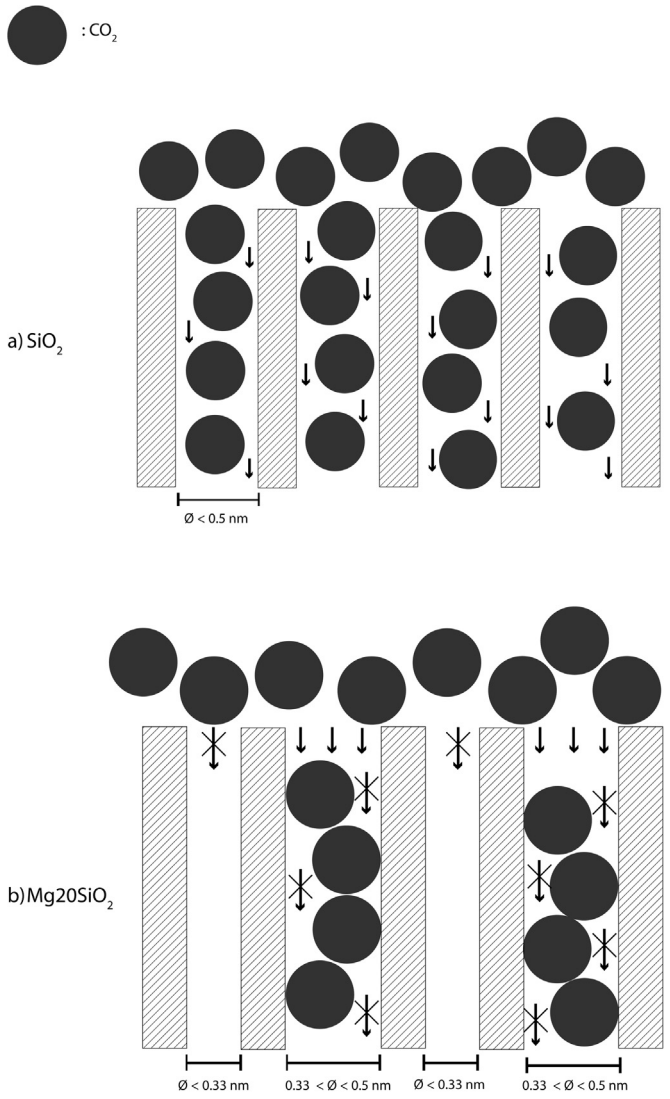

Fig. 7. Schematic presentation of the single gas permeance of CO_2 in pure (a) and 20% Mg-doped silica membrane (b).

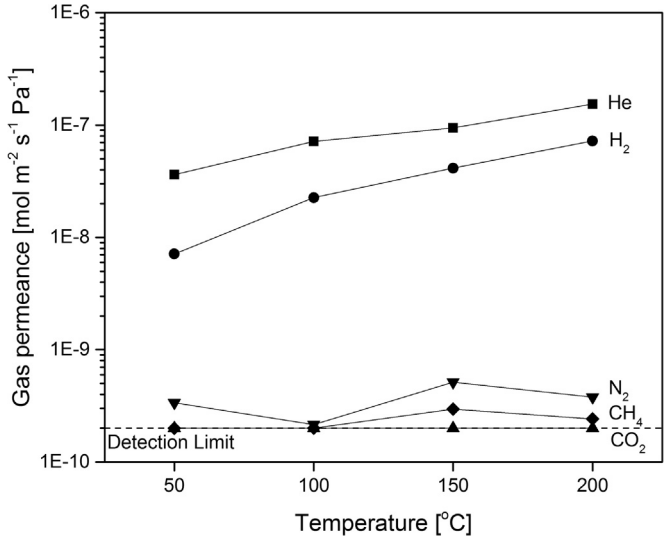

Fig. 8. The gas permeances through 20% Mg-doped membranes at varying temperatures from 50 to 200 °C with a transmembrane pressure of 2 bar (lines are a guide to the eye).

Table 3
The single gas permeances of $Mg20SiO_2$ at temperatures varying from 50 to 200 °C (at a pressure difference of 2 bar).

Temperature [°C]	Gas permeance [10^{-9} mol m^{-2} s^{-1} Pa^{-1}]				
	He	H_2	CO_2	N_2	CH_4
50	36	7.1	*	0.3	*
100	72	23	*	0.2	*
150	95	41	*	0.5	0.3
200	150	72	*	0.4	0.3

* Permeances are below the detection limit of the equipment (0.2 × 10^{-9} mol m^{-2} s^{-1} Pa^{-1}).

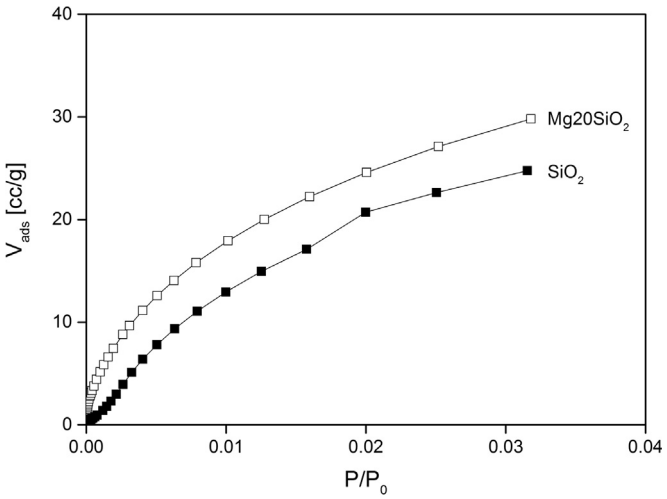

Fig. 9. CO_2 adsorption isotherms of $Mg20SiO_2$ and SiO_2.

saturation pressure of the adsorbate) up to 0.032. The adsorption isotherms are given in Fig. 9.

The adsorption isotherms of SiO_2 and $Mg20SiO_2$ were found to be Type I according to the Brunauer, Deming, and Teller Classification [25] which is suitable for microporous solids. In Type I isotherms, the amount adsorbed is concave to the relative pressure and reaches steady state as $P/P_0 \rightarrow 1$. However, it was not possible to reach P/P_0 values higher than 0.032 in our gas adsorption set-up due to relatively high saturation pressure of CO_2 (26,142 mmHg). From the adsorption isotherms, the Langmuir surface area, which is suitable for monolayer adsorption as seen in microporous solids [26–29], was calculated as 244 and 257 m^2/g for SiO_2 and $Mg20SiO_2$, respectively.

Finally, thermogravimetric analyses were done at 200 °C and the mass uptake was recorded when the gas flow was changed from pure N_2 to CO_2:N_2 (5:2). As a result of CO_2 introduced to the system, the mass changes were calculated and the results are given in Table 4. Although the mass changes were rather low, the mass uptake of CO_2 in 20% Mg-doped silica membranes was 20 times more than that for pure silica. In combination with the CO_2 adsorption experiments this result is an indication that CO_2 adsorption on pure silica is much less than on Mg-doped silica. Besides, this relative low mass change (0.273%) suggests that small amounts of CO_2 could easily block the pores of the 70 nm thick selective layer of 20% Mg-doped silica membranes avoiding

Table 4
Mass uptake on pure and 20% Mg-doped silica powders at 200 °C as a result of CO_2 introduced to the system.

	Mass change [%]
SiO_2	0.014
$Mg20SiO_2$	0.273

further permeation of CO_2 molecules which was clearly shown in single gas permeances.

4. Conclusions

Pure and 10, 15 and 20 mol% Mg-doped microporous silica membranes were fabricated by the sol-gel method, and the gas permeation performance of these membranes were studied extensively. For each composition, four membranes from two different sol sets were prepared, showing only small deviations in gas permeation, indicating reproducible results. Mg doping into the amorphous silica network narrowed the pore size, resulting in a decrease in gas permeances, which is more pronounced for larger size gases such as CO_2, N_2 and CH_4. Therefore, the H_2/CO_2 permselectivity was increased from 9 for pure silica to more than 350 by 20% Mg doping ($Mg20SiO_2$). The H_2/N_2 permselectivity was found to be almost an order of magnitude larger than those of H_2/CO_2 in pure silica and 10 and 15 mol%-Mg doped silica membranes. However, this trend changed for 20% Mg-doped silica, to permselectivity values of 204 and 350 for resp. H_2/N_2 and H_2/CO_2, indicating that the CO_2 permeance is lower than the permeance of the bigger gas N_2. CO_2 trapping, e.g. by preferential adsorption, results in almost no CO_2 permeation through this Mg-doped silica membranes. The difference in CO_2 gas permeances through 15% and 20% Mg-doped silica membranes can be explained by the optimal amount of Mg doping (20%) to create sufficient basic sites on the membrane pores, which causes the adsorption of CO_2 molecules and blocked its further permeance. Study of gas permeance through $Mg20SiO_2$ membrane as function of temperature showed that this membrane exhibits a high CO_2 affinity from 50 °C up to 200 °C. The reversibility of this interaction between CO_2 and Mg-doped silica membrane was tested by performing the permeation of CH_4 both before and after CO_2 permeance. Detecting no decrease in CH_4 permeance after CO_2 permeance tests confirms the reversibility of the interaction.

The Rhodamine-B test and the gas permeation results showed that the pits on the surface of the Mg-doped silica membrane, as observed by SEM, do not reach the intermediate γ-Al_2O_3 layer and therefore there must be an intact separation layer underneath these pits.

The interaction between CO_2 and Mg-doped silica membranes were analysed by thermogravimetric analysis. Upon the change of the gas flow from pure N_2 to N_2-CO_2 mixture, 20% Mg-doped silica was found to have mass uptake of 0.273% which is 20 times higher in pure silica. Even though the adsorbed CO_2 values at 200 °C are rather low, it suggests that very low amount of CO_2 uptake would be sufficient to block the pores of 20% Mg-doped silica for further CO_2 permeation.

More research needs to be conducted into the interaction between the Mg-doped sites and CO_2 that leads to such remarkable increases in H_2/CO_2 permselectivity. Furthermore, a better understanding of the formation of the pits is necessary to help optimizing the performance of Mg-doped silica membranes to have a promising future in industry.

Acknowledgment

This research is supported by the Netherlands Technology Foundation (STW-13941).

References

[1] M. Takht Ravanchi, T. Kaghazchi, A. Kargari, Application of membrane separation processes in petrochemical industry: a review, Desalination 235 (2009) 199–244, http://dx.doi.org/10.1016/j.desal.2007.10.042.

[2] T. Van Gestel, D. Sebold, F. Hauler, W.A. Meulenberg, H.P. Buchkremer, Potentialities of microporous membranes for H_2/CO_2 separation in future fossil fuel power plants: Evaluation of SiO_2, ZrO_2, Y_2O_3–ZrO_2 and TiO_2–ZrO_2 sol–gel membranes, J. Membr. Sci. 359 (2010) 64–79, http://dx.doi.org/10.1016/j.memsci.2010.04.002.

[3] D. Uhlmann, S. Liu, B.P. Ladewig, J.C. Diniz da Costa, Cobalt-doped silica membranes for gas separation, J. Membr. Sci. 326 (2009) 316–321, http://dx.doi.org/10.1016/j.memsci.2008.10.015.

[4] G.R. Gavalas, C.E. Megiris, S.W. Nam, Deposition of H_2-permselective SiO_2 films, Chem. Eng. Sci. 44 (1989) 1829–1835, http://dx.doi.org/10.1016/0009-2509(89)85125-5.

[5] D. Lee, L. Zhang, S.T. Oyama, S. Niu, R.F. Saraf, Synthesis, characterization, and gas permeation properties of a hydrogen permeable silica membrane supported on porous alumina, J. Membr. Sci. 231 (2004) 117–126, http://dx.doi.org/10.1016/j.memsci.2003.10.044.

[6] H.Y. Ha, S.W. Nam, S.-A. Hong, W.K. Lee, Chemical vapor deposition of hydrogen-permselective silica films on porous glass supports from tetraethylorthosilicate, J. Membr. Sci. 85 (1993) 279–290, http://dx.doi.org/10.1016/0376-7388(93)85281-Z.

[7] M. Nomura, H. Aida, S. Gopalakrishnan, T. Sugawara, S.-i. Nakao, S. Yamazaki, et al., Steam stability of a silica membrane prepared by counter-diffusion chemical vapor deposition, Desalination 193 (2006) 1–7, http://dx.doi.org/10.1016/j.desal.2005.08.019.

[8] R.M. de Vos, H. Verweij, High-selectivity, high-flux silica membranes for gas separation, Science 279 (1998) 1710–1711, http://dx.doi.org/10.1126/science.279.5357.1710.

[9] K. Kusakabe, S. Sakamoto, T. Saie, S. Morooka, Pore structure of silica membranes formed by a sol–gel technique using tetraethoxysilane and alkyltriethoxysilanes, Sep. Purif. Technol. 16 (1999) 139–146, http://dx.doi.org/10.1016/S1383-5866(98)00120-8.

[10] D.-W. Lee, S.-E. Nam, B. Sea, S.-K. Ihm, K.-H. Lee, Synthesis of silica membranes on a porous stainless steel by sol-gel method and effect of preparation conditions on their permselectivity, Bull. Korean Chem. Soc. 25 (2004) 1371–1378, http://dx.doi.org/10.5012/bkcs.2004.25.9.1371.

[11] A. Ayral, A. Julbe, V. Rouessac, S. Roualdes, J. Durand, Microporous silica membrane: basic principles and recent advances, in: R. Mallada, M. Menendez (Eds.), Membr. Sci. Technol., 2008, pp. 33–79. https://dx.doi.org/10.1016/S0927-5193(07)13002-3.

[12] M. Kanezashi, K. Yada, T. Yoshioka, T. Tsuru, Design of silica networks for development of highly permeable hydrogen separation membranes with hydrothermal stability, J. Am. Chem. Soc. 131 (2009) 414–415, http://dx.doi.org/10.1021/ja806762q.

[13] R.M. de Vos, H. Verweij, Improved performance of silica membranes for gas separation, J. Membr. Sci. 143 (1998) 37–51, http://dx.doi.org/10.1016/S0376-7388(97)00334-7.

[14] R. Igi, T. Yoshioka, Y.H. Ikuhara, Y. Iwamoto, T. Tsuru, Characterization of Co-doped silica for improved hydrothermal stability and application to hydrogen separation membranes at high temperatures, J. Am. Ceram. Soc. 91 (2008) 2975–2981, http://dx.doi.org/10.1111/j.1551-2916.2008.02563.x.

[15] M. Kanezashi, S. Miyauchi, H. Nagasawa, T. Yoshioka, T. Tsuru, Gas permeation properties through Al-doped organosilica membranes with controlled network size, J. Membr. Sci. 466 (2014) 246–252, http://dx.doi.org/10.1016/j.memsci.2014.04.051.

[16] H. Qi, J. Han, N. Xu, Effect of calcination temperature on carbon dioxide separation properties of a novel microporous hybrid silica membrane, J. Membr. Sci. 382 (2011) 231–237, http://dx.doi.org/10.1016/j.memsci.2011.08.013.

[17] M. ten Hove, A. Nijmeijer, L. Winnubst, Facile synthesis of zirconia doped hybrid organic inorganic silica membranes, Sep. Purif. Technol. 147 (2015) 372–378, http://dx.doi.org/10.1016/j.seppur.2014.12.033.

[18] A. Nijmeijer, Hydrogen-Selective Silica Membranes for Use in Membrane Steam Reforming (Ph.D. thesis), University of Twente, 1999.

[19] V. Boffa, J.E. ten Elshof, R. Garcia, D.H.A. Blank, Microporous niobia–silica membranes: Influence of sol composition and structure on gas transport properties, Microporous Mesoporous Mater. 118 (2009) 202–209, http://dx.doi.org/10.1016/j.micromeso.2008.08.038.

[20] K. Yoshida, Y. Hirano, H. Fujii, T. Tsuru, M. Asaeda, Hydrothermal stability and performance of silica-zirconia membranes for hydrogen separation in hydrothermal conditions, J. Chem. Eng. Jpn. 34 (2001) 523–530, http://dx.doi.org/10.1252/jcej.34.523.

[21] M.J. Ramírez-Moreno, I.C. Romero-Ibarra, J. Ortiz-Landeros, H. Pfeiffer, Alkaline and alkaline-earth ceramic oxides for CO_2 capture, separation and subsequent catalytic chemical conversion, in: C.R.V. Morgado, V.P.P. Esteves (Eds.), CO_2 Sequestration and Valorization, 2014, pp. 403–441. https://dx.doi.org/10.5772/57444.

[22] M.K. Ram Reddy, Z.P. Xu, G.Q. Lu, J.C. Diniz da Costa, Layered double hydroxides for CO_2 capture: Structure evolution and regeneration, Ind. Eng. Chem. Res. 45 (2006) 7504–7509, http://dx.doi.org/10.1021/ie060757k.

[23] R.S.A. de Lange, J.H.A. Hekkink, K. Keizer, A.J. Burggraaf, Formation and characterization of supported microporous ceramic membranes prepared by sol-gel modification techniques, J. Membr. Sci. 99 (1995) 57–75, http://dx.doi.org/10.1016/0376-7388(94)00206-E.

[24] J.C. Diniz da Costa, G.P. Reed, K. Thambimuthu, High temperature gas separation membranes in coal gasification, Energy Procedia 1 (2009) 295–302, http://dx.doi.org/10.1016/j.egypro.2009.01.041.

[25] K.S.W. Sing, D.H. Everett, R.A.W. Haul, L. Moscou, R.A. Pierotti, J. Rouquérol, et al., Reporting physisorption data for gas/solid systems with special reference to the determination of surface area and porosity, Pure Appl. Chem. 57 (1985) 603–619, http://dx.doi.org/10.1351/pac198557040603.

[26] X. Gao, J.C. Diniz da Costa, S.K. Bhatia, Adsorption and transport of gases in a supported microporous silica membrane, J. Membr. Sci. 460 (2014) 46–61, http://dx.doi.org/10.1016/j.memsci.2014.02.028.

[27] B. Bettens, A. Verhoef, H.M. van Veen, C. Vandecasteele, J. Degrève, B. Van Der Bruggen, Adsorption of pure vapor species on microporous silica membranes and silica pellets, J. Phys. Chem. C 114 (2010) 9416–9423, http://dx.doi.org/10.1021/jp101600t.

[28] B.L. Newalkar, S. Komarneni, Synthesis and characterization of microporous silica prepared with sodium silicate and organosilane compounds, J. Sol-Gel Sci. Technol. 18 (2000) 191–198, http://dx.doi.org/10.1023/A:1008782117894.

[29] T. Yoshioka, E. Nakanishi, T. Tsuru, M. Asaeda, Experimental studies of gas permeation through microporous silica membranes, AIChE J. 47 (2001) 2052–2063, http://dx.doi.org/10.1002/aic.690470916.